

Supporting Information: Ionic Charge Distributions in Silicon Atomic Surface Wires

Jeremiah Croshaw^{1,2}, Taleana Huff³, Mohammad Rashidi¹, John Wood¹, Erika Lloyd¹, Jason Pitters³,
Robert Wolkow^{1,2,3}

¹Department of Physics, University of Alberta, Edmonton, Alberta, T6G 2J1, Canada

²Quantum Silicon Inc., Edmonton, Alberta, T6G 2M9, Canada

³Nanotechnology Research Centre, National Research Council Canada, Edmonton, Alberta, T6G 2M9,
Canada

Figures S1 to S14 as mentioned in the text

Supporting Discussions for the bare dimer, and charge distributions among DB wires.

Experimental Methods

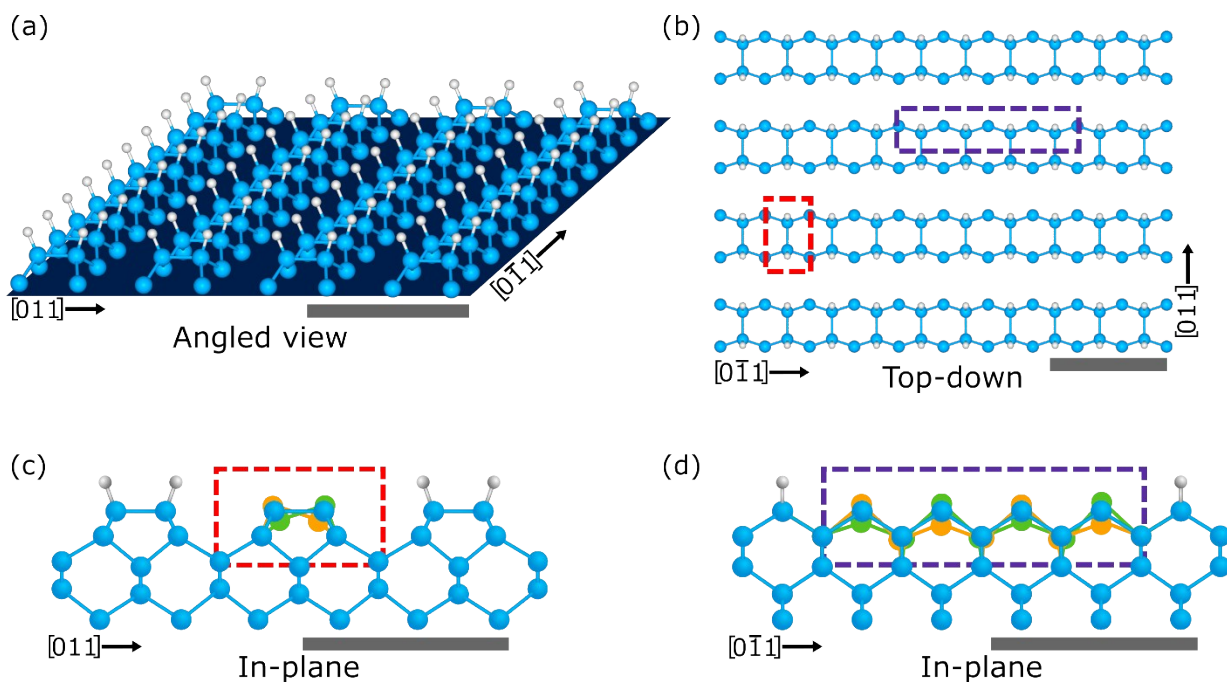


Figure S1. **Crystallographic details.** Ball and stick models of the H-Si(100)-2x1 surface in an angled (a) and top (b) view highlighting the different crystal geometry along the $[011]$ and $[0\bar{1}1]$ direction. A (hydrogen terminated) dimer structure is indicated with the red box in (b) while a (hydrogen terminated) four DB wire is highlighted with the purple box in (b). (c) A side view of the surface along the $[011]$ direction showing the (hydrogen desorbed) dimer configuration. The green and orange structure show a lattice distortion corresponding to the degenerate (+/-+, du/ud) configurations for a bare dimer as mentioned in the main text. Lattice geometry extracted from ref. ¹. (d) A side view of the surface along the $[0\bar{1}1]$ direction showing the (hydrogen desorbed) four DB wire configuration. The green and orange structures show a distorted lattice configuration corresponding to the degenerate (0-+/-+-0, dudu/udud) configuration of the four DB wire. Lattice geometry is approximated from Ref. ² and Ref. ³. Scale bars are 1 nm.

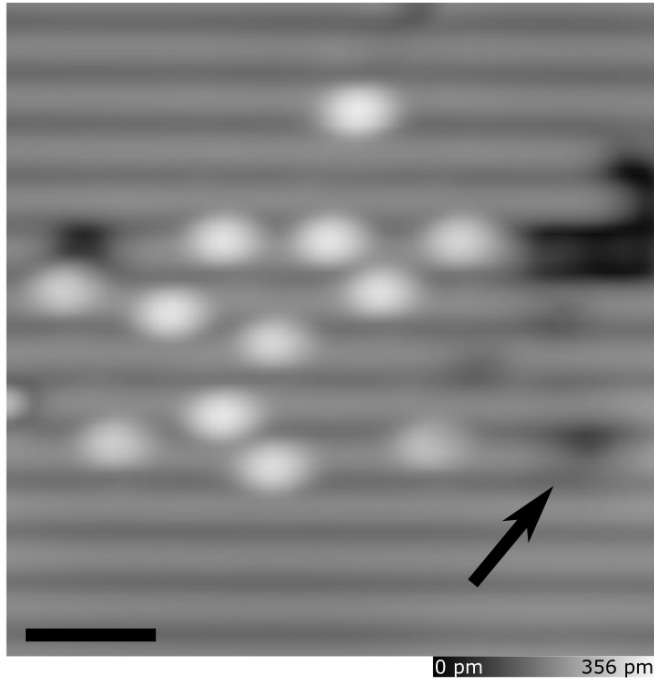


Figure S2. **Cluster of surface DBs.** Filled states image (-1.8 V) of the area surrounding the DB from Figure 1 (marked by black arrow). Scale bar is 2 nm.

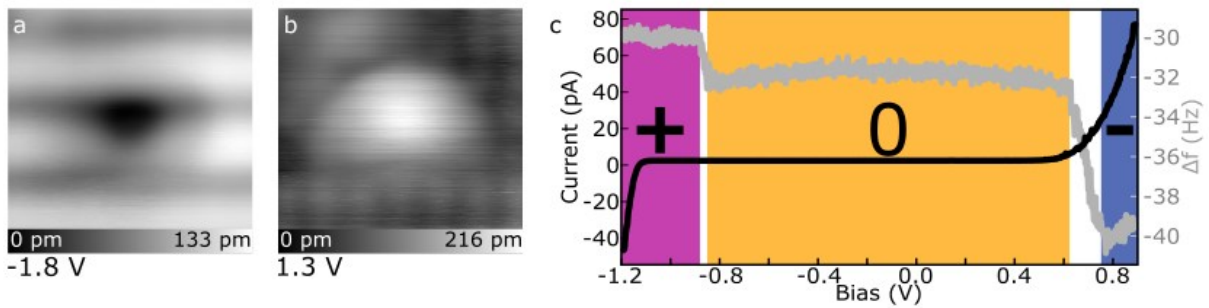


Figure S3. **STM measurements of the single DB.** (a) The filled states image of the DB. (b) The empty states image of the DB. Sample biases are indicated in the lower left of each image. Each image is $2.6 \times 2.6 \text{ nm}^2$ (c) $I(V)$ spectroscopy of the DB compared to the $\Delta f(V)$ spectroscopy (in grey) from the main text. The empty and filled states images in (a) and (b) better match the characteristics of a DB on a p-type sample suggesting the nearby electrostatic perturbations have significantly modified the emptying and filling rates of the DB^{4,5} rendering it positive at -1.8 V and neutral at 1.3 V as opposed to the expected neutral (-1.8 V) and negative (1.3 V) charge state commonly observed on n-type samples⁶.

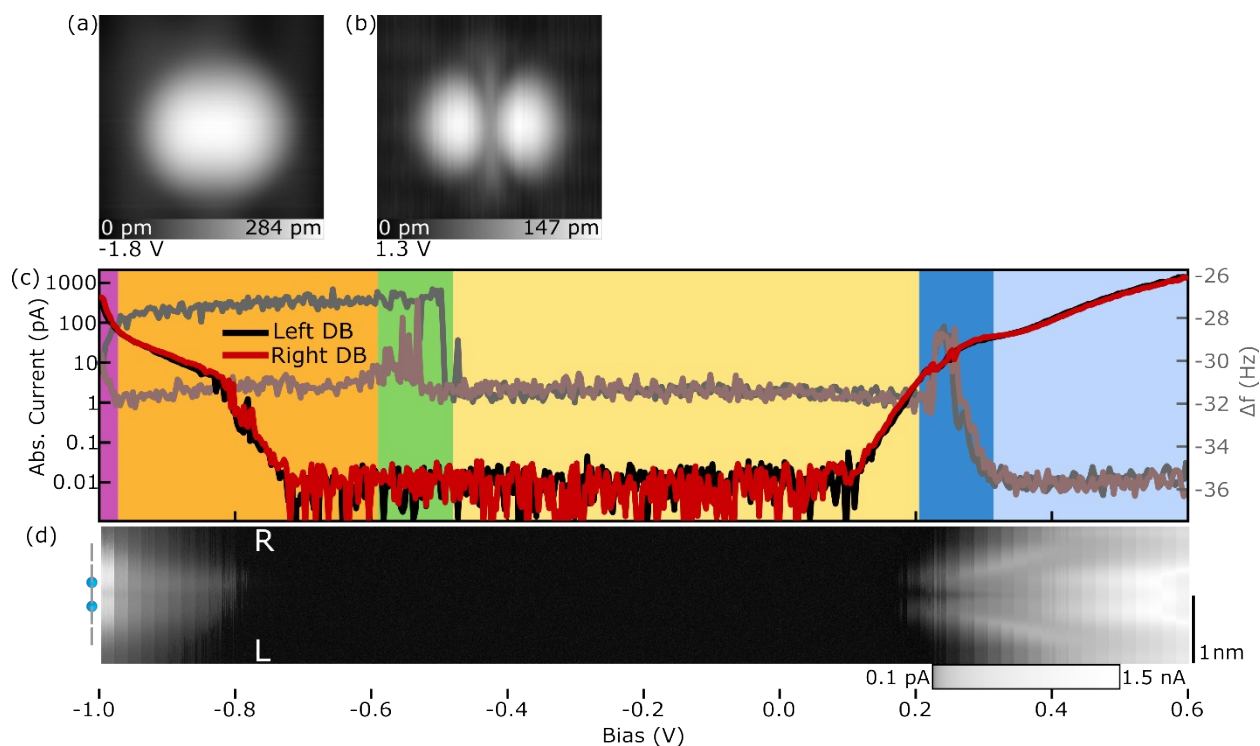


Figure S4. Bare dimer constant current and Δf maps. (a) filled (-1.8 V) and (b) empty (1.3 V) states STM image of the bare dimer structure. (c) $I(V)$ spectroscopy of the bare dimer compared to the $\Delta f(V)$ spectroscopy from the main text. (f) $I(V)$ line scan maps simultaneously measured with the $\Delta f(V)$ line scan maps in Figure 2 (f). The position of the bare dimer in the line scans is indicated on the left of (d) with the grey line added to orient the structure. 50 line scans at bias increments of 0.02 V are shown. The current scale in (c) and (d) is plotted logarithmically to highlight low current features at the onset of the conduction and valence band. Relative heights for each are -300 pm. The scale bar for the line scans is 1 nm as indicated on the right (d).

The Bare Dimer

The bare dimer offers a unique structural formation compared to other DB structures of the H-Si(100) surface due to the presence of a dimer bond. As outlined in the main text, this unique structural property results in six discernable regions within the probed bias range. By looking at the $\Delta f(V)$ spectroscopies over both DBs in both forward and backward scan directions, and at various tip-sample separations as shown in Figure S5, further insights into the structural and charge states of the bare dimer can be gained. The left panel shows the $\Delta f(V)$ spectroscopies over the left DB with the forward direction indicating a bias sweep from -1.0 V to 0.6 V (0.6 V to -1.0 V for the backward direction) while the right panel shows spectroscopies over the right DB. Each spectrum is taken between -200 pm and -350 pm with 50 pm increments. The spectra with more negative Δf signals correspond to a reduced tip-sample separation due to an increased covalent interaction between the tip and sample. The spectroscopy features corresponding to each of the six bias windows are visible for all heights with a slight variation in their onset due to the variation in tip induced band bending with changing heights. One of the key differences seen between the left and right DB occurs in the orange, green, and yellow

regions. In the yellow region, there is a hysteresis seen between the forward and backward scans of the left DB that is not seen in the right DB. As the tip probes the left DB within the yellow region in the forward direction, the DB transitions from positive to negative on the time order of a few seconds. Scanning in the backward direction, the left DB stays in the negative charge state until the bias reaches values within the green and orange region. The length at which the left DB stays in the positive state before transitioning to the negative state in the yellow region decreases with reduced tip height suggesting it is influenced by a stronger interaction with the tip. With the exception of a short-lived transition to the positive charge state at -250 pm, the right DB does not show this hysteresis between the forward and backward directions, remaining instead in the negative charge state.

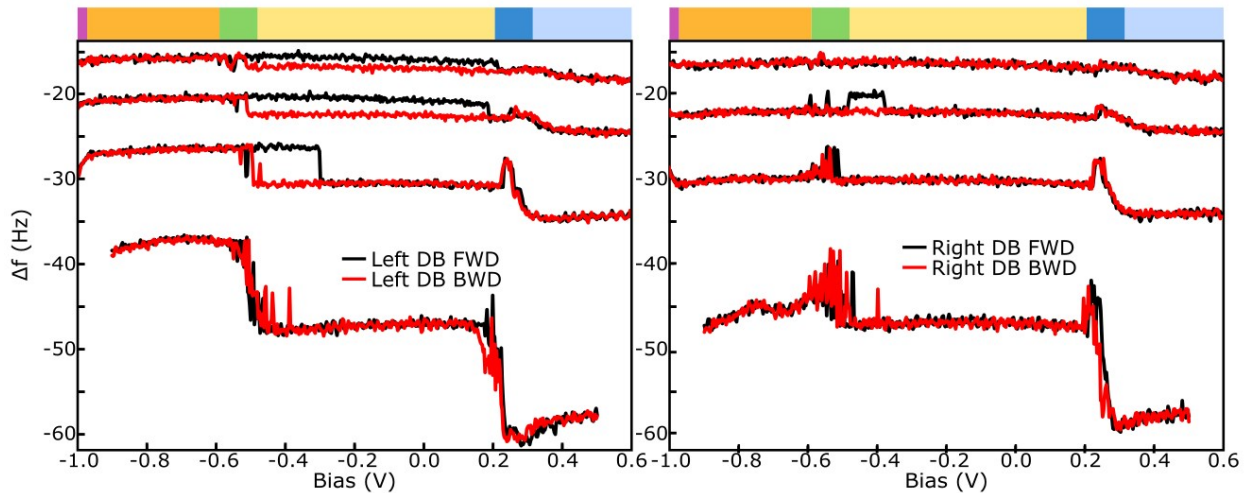


Figure S5. **The Bare Dimer $\Delta f(V)$ Spectroscopies.** $\Delta f(V)$ spectroscopy over the left and right DB as indicated. The black curves show the forward scan direction (-1.0 V to 0.6 V) while the red curves show the backward direction (0.6 V to -1.0 V). Each spectroscopy over the left and right DB are taken at different heights corresponding to a tip offset of -200 pm (less negative Δf), -250 pm, -300 pm, and -350 pm (more negative Δf). The bias regions mentioned in the text are coloured above each panel.

To better understand the influence of the tip within this bias region, it is useful to consider the electron energy levels of the left and right DB as a function of the nuclear coordinates of the host Si atom relative to the surface⁷⁻⁹. Figure S6 (a) shows the double potential well of the two DBs in a bare dimer. In this instance, the left DB (drawn in red) is shown in the positive charge state with the more sp^2 -like character of the host Si atom indicated by the leftward shift along the horizontal axis. The right DB (black) is shown in the negative charge state as indicated by the presence of two electrons (black arrows) with the more sp^3 -like character represented by the rightward shift in the nuclear coordinate. The horizontal dashed lines within the potential indicate possible electron levels available through an electron-phonon coupling^{8,9}. The observed charge state of each DB is facilitated by the emptying and filling rates between each DB and the conduction band, the DBs and the tip, and between the DBs of the bare dimer as indicated with the grey arrows. The coloured regions are the same as the main text and are used to reference the position of the tip Fermi level.

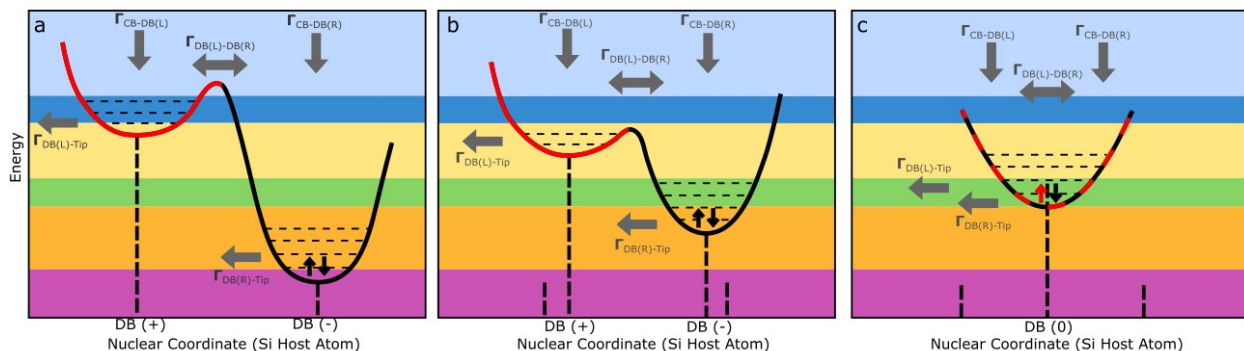


Figure S6 The bare dimer charge states with atom position. (a) Qualitative double potential well system of the buckled bare dimer showing the left DB (red) in the positive charge state and the right DB (black) in the negative charge state. The difference in charge state is accompanied by different nuclear coordinates of the host silicon atom indicated along the horizontal axis. The coloured regions match those presented in the spectroscopies of the main text and SI figures which are used to reference the position of the tip Fermi level. The grey arrows indicate potential current pathways between the conduction band and the DBs, the DBs and the tip, and between DBs. The horizontal lines within the potential well indicate possible electron energy levels made available through electron-phonon coupling. (b) The same potential well in (a) except an attractive interaction between the tip and left DB has shifted the nuclear coordinates of the host Si atom corresponding to a shift in energy level for each DB. The original lattice position is shown by the two shorter vertical dashed lines. (c) The double potential well system of the symmetric bare dimer where both DBs now sit at the same relative nuclear coordinate resulting in the energetic alignment of the two energy levels.

To appreciate the dynamics within the yellow region, consider a tip positioned above the left (positive) DB. The attractive interaction from the tip raises^{10–12} the host Si atom from the surface changing the nuclear coordinate in both the left and right DB as indicated in Figure S6 (b). With a reduced separation in energy between the filled, negative DB and the empty, positive DB, it becomes possible for an electron to thermally excite to the left DB leaving the bare dimer in an unbuckled, symmetric configuration shown in Figure S6 (c). Following this excitation, the bare dimer then buckles again to the ionic (-+, ud) configuration. Due to the interaction of the tip, the left DB now preferentially buckles to host the negative charge. If the tip is positioned over the negative DB in the bare dimer (right DB or the left DB in the backward direction), the charge transition from a negative to positive DB does not occur. The additional interaction from the tip attracts the DB, keeping it in a preferred sp^3 configuration, preventing an electron from transferring to the positive DB which would unbuckle the dimer. As mentioned in the main text, the preferred configuration of the buckled bare dimer is likely dictated by some unseen electrostatic perturbation in the subsurface region. It is important to emphasize that during this transition, the Fermi level of the tip never drops below the energy level of the negative DB and so all the electron dynamics within the bare dimer are solely due to the movement of charge within the bare dimer. Additionally, if the tip position is allowed to laterally move from the negative DB to the positive DB within the bare dimer, (as in the Δf line scan maps), it allows for the bare dimer to buckle between the two degenerate configurations. The likelihood of a transition is dictated by tip height with larger tip sample separations resulting in fewer transitions and smaller tip sample separations resulting in more transitions as shown in Figure S7.

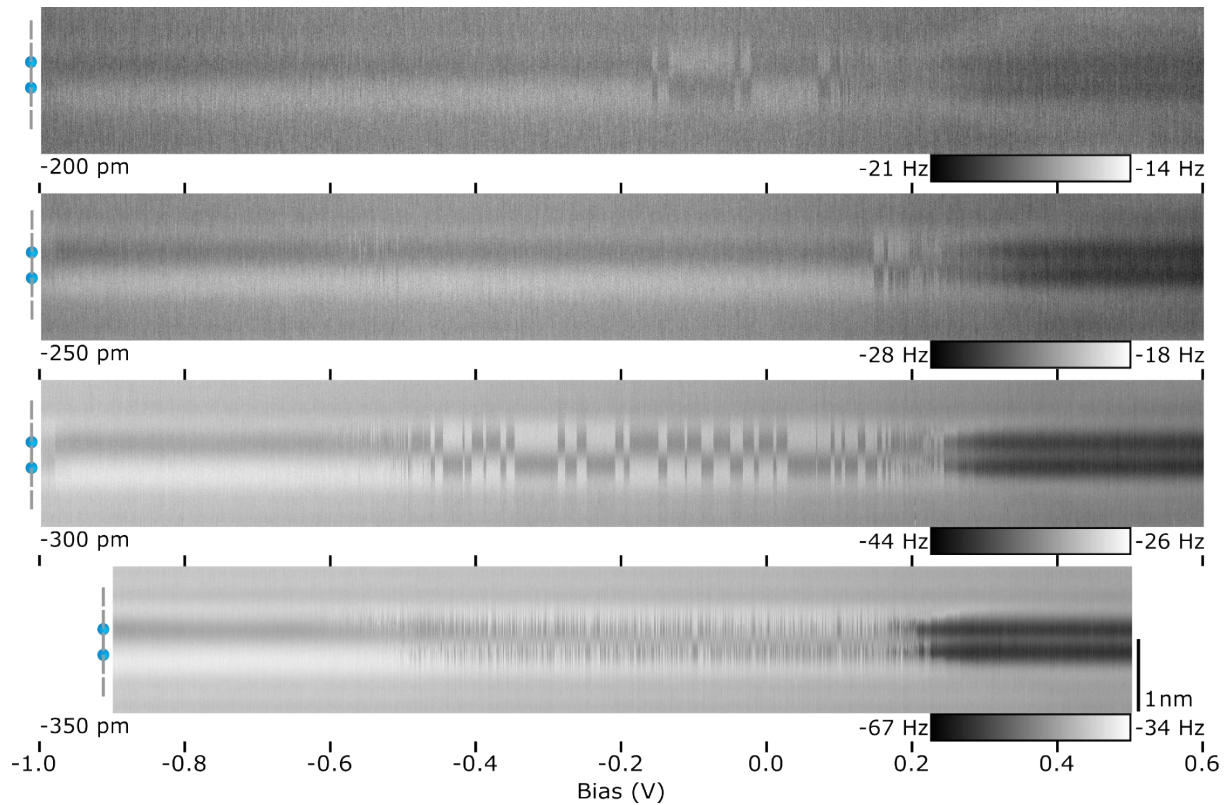


Figure S7 **The bare dimer $\Delta f(V)$ line scan maps at various tip heights.** Imaging parameters are the same as Figure 2 (b). The relative tip height is indicated in the lower left corner of each line scan map.

Looking at the green region of Figure S5, the rapid switching in Δf can be seen in both the left and right DB in the forward and backward directions suggesting that the dynamics seen are not dependent on tip position over the bare dimer. We attribute this rapid switching between states to the resonance of the unbuckled pi state of the bare dimer with the Fermi level of the tip. The dynamics are then dictated by the competing emptying rates from the DB to the tip ($\Gamma_{DB(R/L)-Tip}$) and the filling rates from the conduction band to the DB ($\Gamma_{CB-DB(R/L)}$) as well as the charge transfer between the DBs ($\Gamma_{DB(R/L)-DB(L/R)}$), and corresponding buckling and unbuckling associated with charge localization within the bare dimer. It is currently unknown what mechanism drives the bare dimer into the symmetric configuration since such signals are seen over both the positive and negative DB. Correlating the reduction in frequency of such switching signals to increased tip sample separations, it is possible the bare dimer dynamics could be facilitated by the oscillation of the AFM tip, however, further studies are needed to support this claim.

Lastly, the orange region shows the absence of switching between charge states with the left DB imaging as positive and the right DB imaging as negative in both the forward and backward direction. Looking at Figure S6 (a), it can be seen that the Fermi level of the tip is now between the proposed electron energy levels of the symmetric bare dimer and the electron levels of the fully buckled negative DB. Much like the yellow region, interactions with the tip would change the electron energy level of the negative DB due to tip induced variations to the nuclear coordinate. The difference is that within the

orange region, the electrons within the negative DB would be emptied to the tip before the bare dimer reaches its symmetric configuration. If the subsequent filling rate from the conduction band is quicker than any lattice distortion and charge redistribution within the bare dimer, it follows that no switching of the bare dimer configuration would occur. This claim is supported by the observation of current at roughly -0.75 V in Figure S4 (c) with no modification to the charge state in the Δf signal seen in the background of Figure S4 (c). Investigating the dynamics of such emptying and filling rates are outside the abilities of conventional STM and nc-AFM and warrant further investigation using time-resolved techniques.

Insights into the purple, dark blue, and light blue region can also be gained from looking at Figure S6. In the purple region, the Fermi level of the tip is now below the energy level of the fully buckled negative DB allowing for a constant emptying of this state. Although the constant height image in the bias range shows the bare dimer in a symmetric configuration, the proposed energy alignment of the bare dimer with the Fermi level of the tip suggests that it sits in a (0+) configuration that may buckle between the (0+/-0) configurations at a rate faster than the AFM sampling rate giving the symmetric appearance in the Δf images. The dark blue and light blue regions now bring the energy level of the positive DB in alignment with the Fermi level of the tip indicating that this electron level may now be filled by the tip. The unique features seen in the $\Delta f(V)$ spectroscopies and line scans maps corresponding to the sharp increase in Δf and sudden decrease following the transition from the dark blue to the light blue region suggest a combination of lattice and charge dynamics outside the sampling rates of our STM and AFM and warrant subsequent investigation. As mentioned in the main text, the more negative shift in Δf likely corresponds to a net charging of the DB structure, but charge dynamics make it difficult to assess if the DB structure is rapidly switching between a net $1e^-$ (0-/-0) charge configuration or sits in a $2e^-$ (-) configuration.

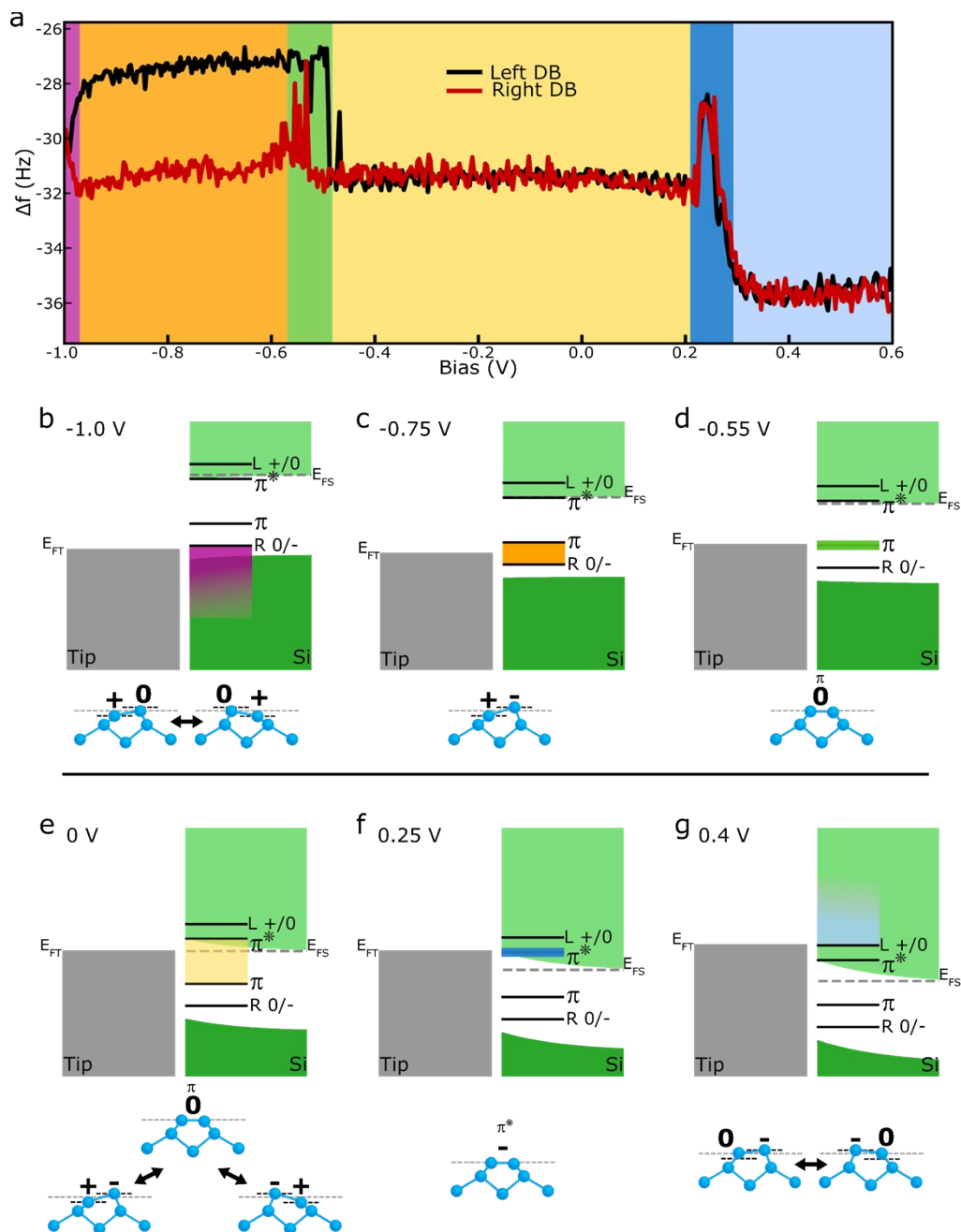


Figure S8. **Band diagrams for the associated $\Delta f(V)$ spectroscopies of a bare dimer.** (a) The $\Delta f(V)$ spectroscopy of a bare dimer as shown in Figure 2 of the main text. (b)-(g) The associated predicted band diagrams of the bare dimer system at bias values indicated in the top left of each panel. The bulk Si band diagrams were calculated using semi-tip¹³. The ball and stick images show the expected lattice and charge distribution as discussed with Figure S6. It is important to note that the π and π^* states drawn in the band diagrams are only available when the bare dimer is in a symmetric configuration and the $L +/0$ ($+$ to 0) and $R 0/-$ (0 to $-$) charge transition levels only exist when the bare dimer is in the buckled configuration.

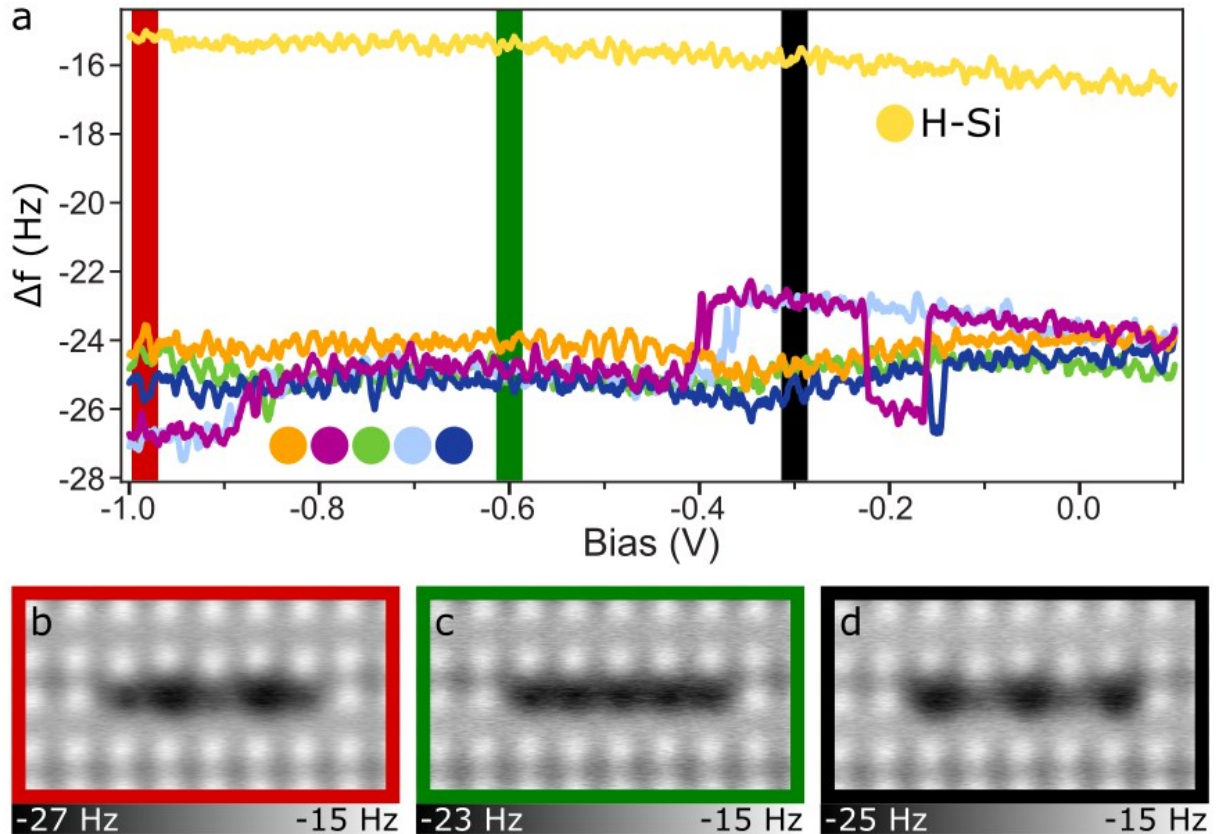


Figure S9: Net positive configuration of a 5 DB wire as probed with an H terminated tip.

(a) $\Delta f(V)$ spectra taken over each DB in the 5 DB wire as indicated in the lower left, as well as over the hydrogen surface in yellow (tip height = -280 pm). A Savitsky-Golay filter of order 9 was applied to allow easier differentiation of the curves. (b-d) Constant-height Δf AFM images of the wire with bias values as indicated in (a). Each image is 1.9×3.4 nm² with a relative tip height of -310 pm. The presence of a net positive lattice distribution in DB wires was not as easily observed for results presented in the main text due to an increase in current from the valence band at the onset of the net positive charge transition associated with a different alignment of the DB energies with the Fermi level of the crystal due to varying sample preparations¹⁴. Charge transitions correlated to the net positive distribution can be seen for the 5 and 7 DB case in Figure S11 but are short lived due to the onset of sustained tunneling current (not shown). Further studies on p-type crystals using a Si terminated AFM tip would be useful to better demonstrate the net positive redistribution of DB wires.

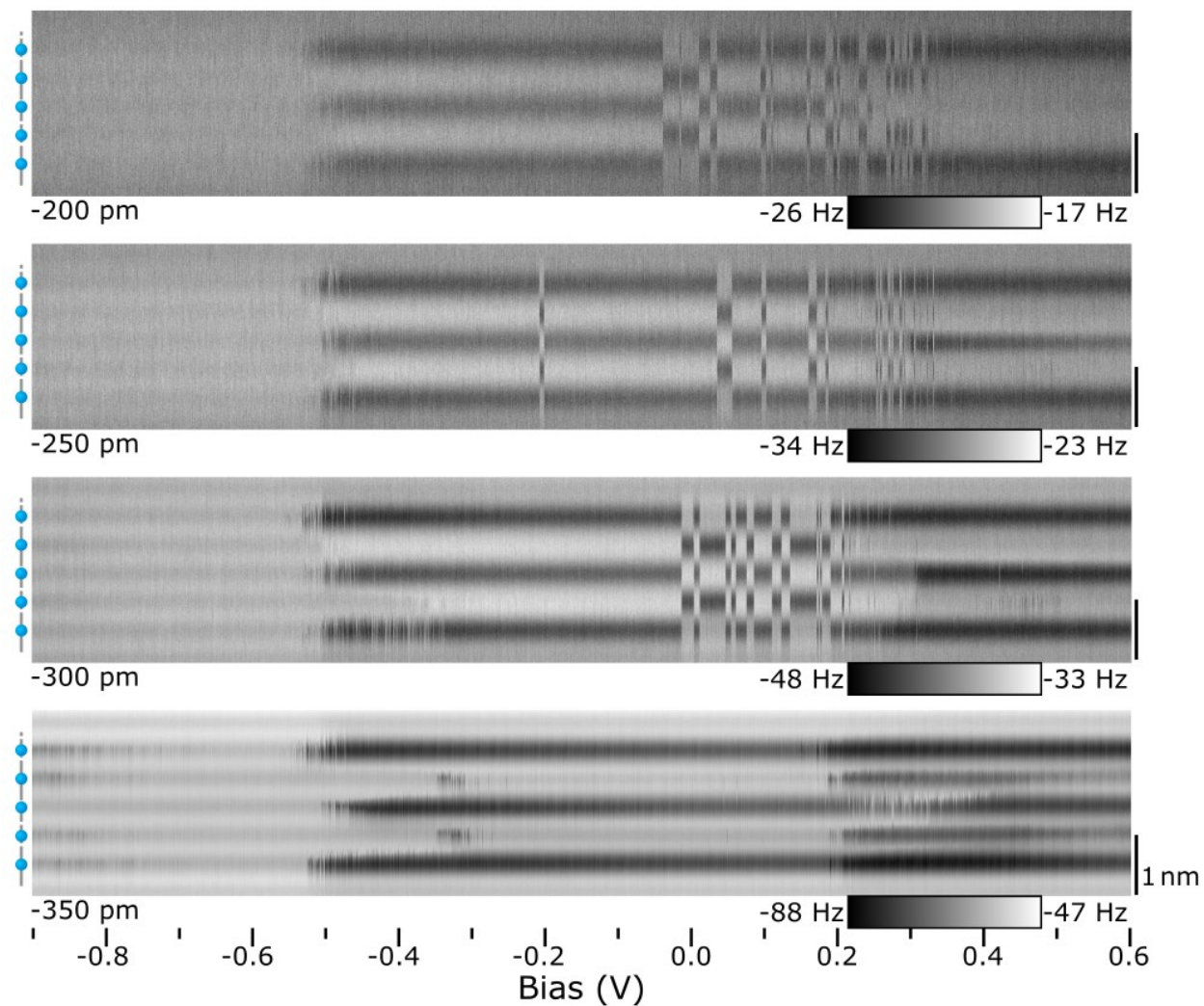


Figure S10. **Charge distribution with tip height.** Line scans of a 5 DB wire. Bias increments are 0.02 V with 50 line scans taken at each bias. Each image is taken at a different relative depth as indicated in the bottom left of each set of scans. The streakiness of the centre DB at -350 pm is dependent on scan direction which in this case is top to bottom.

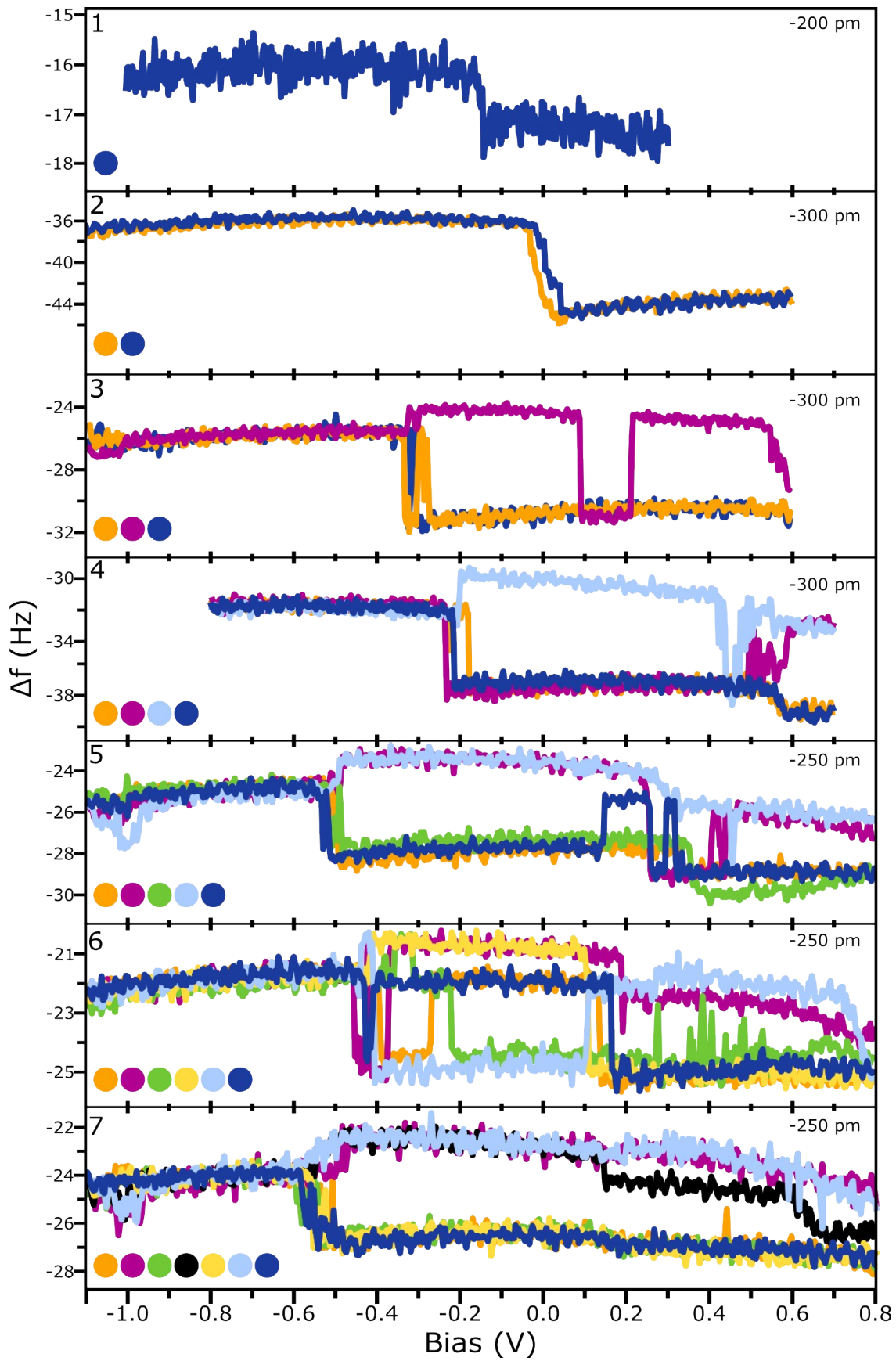


Figure S11. **KPFM Spectroscopy of DB Wires.** $\Delta f(V)$ spectroscopy over DB wires length 1 to 7 as indicated in the top left of each panel. Spectroscopy colors are shown in the bottom left of each panel. The height of each spectroscopy is indicated in the top right and was chosen to highlight the charge switching of each DB without significant influence from the tip. Note that the centre DB of the 3 DB wire briefly enters a (-) charge state as mentioned in the text. Since neither the left or right DB enter the expected neutral state, the middle DB is thought to only enter this higher energy state due to the sustained interaction with the tip as discussed in the main text.

Charging Biases and DB wires of Greater Length

As discussed in the main text, the energy at which each wire transitions from the net neutral to net negative ($1e^-$) charge state depends on the wire length with longer wires ionizing at lower sample biases as predicted in Ref^{2,15}. Figure S12 highlights the first ionization bias for DB wires length 2 to 7, along with the second ionization bias where a wire can facilitate an additional negative charge. The 2 DB wire undergoes the first ionization at the largest sample bias around -0.08 V while the 7 DB wire is ionized at -0.5 V. A similar trend can be seen when looking at the secondary ionization energy transitioning to a multiple negative charge state in DB wires as shown in Figure S12. As the sample bias increases and the DB wire is forced to accept an additional charge from the tip, the DB wires redistribute their charge so that the separation between negative charges is maximized. This is most easily observed for the 4 and 5 DB wire case which now contain two negative DBs located at the wire edges with all middle DBs imaged in the neutral charge state. The 6 and 7 DB wires also readjust to hold a negative charge in both wire ends. The 7 DB wire easily accommodates the addition of the negative charge by neutralizing the centre DB leaving two (-+, udu) clusters at the ends of the wire. The 6 DB wire appears to be in a more frustrated configuration with both outer DBs appearing negative and the two inner DBs showing a switching behaviour similar to the 2 DB case. It is likely that this DB cluster is switching between a degenerate (-+00-/00+-) charge distribution as the tip scans over the wire although confirmation of such a configuration is outside the available sampling rates.

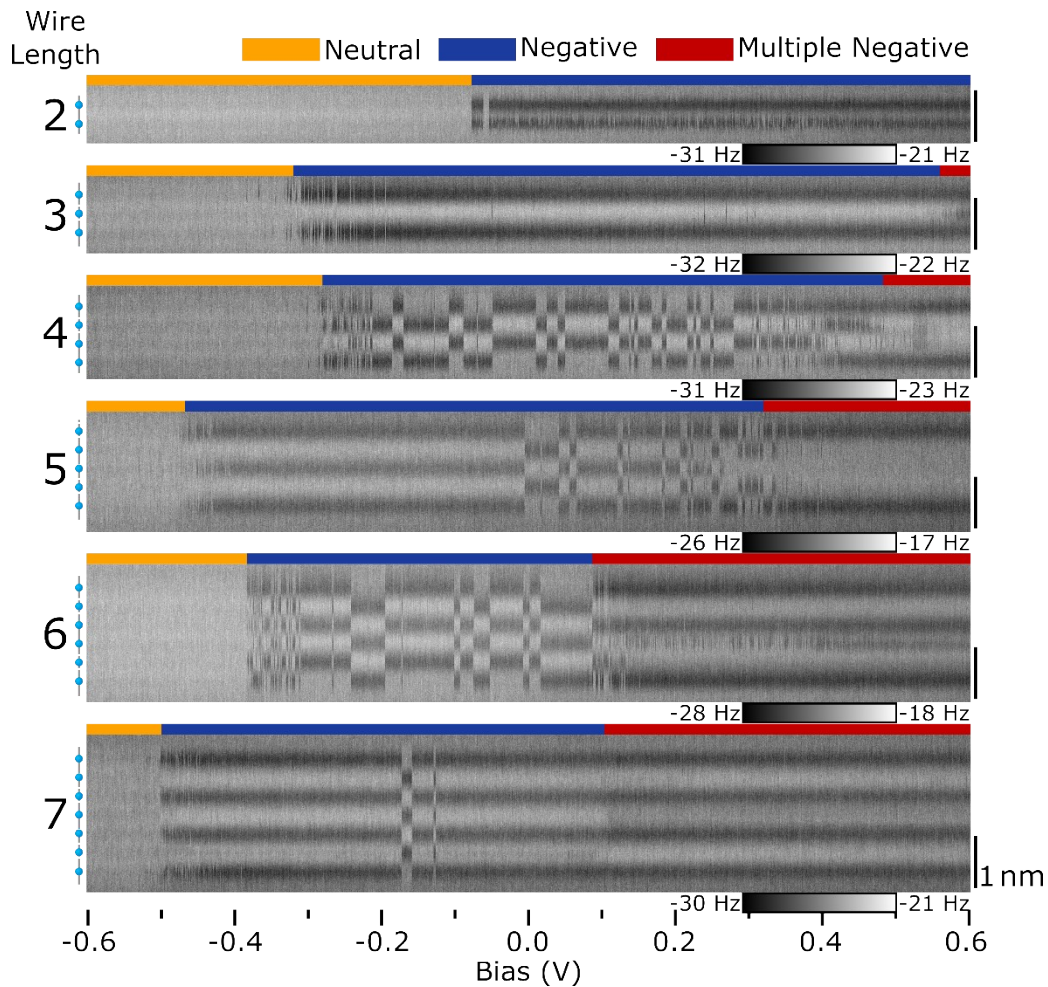


Figure S12. **Charging of DB wires.** Line scans of DB wires length 2 to 7. Bias increments are 0.02 V with 50 line scans taken at each bias. Orange indicates the bias window when the DB wire is neutral, blue indicates a single negative charge in either the lower or higher order (odd) or degenerate (even) configuration, and red indicates an observed charge greater than -1. The position of each DB in the DB wires is indicated to the left of each line scan in blue. Line scans taken for DB wires of length 2,4,6 and 7 were taken at -250 pm, 3 was taken at -300 pm, 5 was taken at -200 pm. These heights were selected for each wire to minimize the effects of tip induced switching due to differing tip character from multi day measurements.

As the DB length is increased, the DB wires can more easily accommodate a greater number of charges. Since this added charge introduces an additional polaronic effect¹⁶⁻¹⁹, the DB wires are able to reorder into a greater number of configurations which are stabilized by this added charge. Figure S13 shows select Δf maps of DB wires length 8 to 15 at 0 V. At this bias, the 8 DB wire has transitioned from the (u...d) configuration expected for even wires and instead features two (-+-) clusters at either end. The (u...d/d...u) configuration for the 8 DB wire can be seen in the line scans of Figure S14 at bias values lower than the configuration seen in Figure S13 (a), suggesting that the configuration shown in Figure S13 (a) is a higher energy configuration. The 9 DB wire of Figure S13 (b) is shown to switch between two configurations mid-scan. The position of the (-+-) cluster on the left side of the 9 DB wire shifts one lattice site with the middle DB appearing negative only when the (-+-) cluster is at the end of the DB

wire. Its appearance is very similar to the 5 DB wire at reduced tip sample separation suggesting this DB may only be negative due to a tip interaction. The right side of the 9 DB structure does not appear to switch with the left side of the wire which supports the claim that the added polaronic effect from additional charge can stabilize the wires into higher energy configurations, allowing for the wires to decouple into smaller subunits. The 10 DB wire again features (-+-) clusters at the edges of the wire with the central two DBs appearing negative. The line scans in Figure S14 again reveal that this is a higher energy configuration compared to the (ud/du) configuration expected with even length DB wires. The shape of the two central DBs appear much more asymmetric compared to all other negative DBs seen suggesting that this is likely a single negative DB which switches between the middle left and middle right DB due to a tip induced charging (like the 2 and 6 DB wire cases), resulting in a net charge of $3e^-$ for the 10 DB wire at 0 V. The 11 DB wire shows both (-+-) clusters at the ends of the wires with 2 negative DBs separated by a neutral DB giving the structure an apparent charge of $4e^-$.

The DBs of length 12 to 15 show similar trends as observed in DB wires of previous lengths. The 12 and 15 DB wires both show a switching of the charge configuration within the wire with a decoupling of the left and right sides. The 13 and 14 DB wires appear to be in a stable configuration with the centre DB imaging very similar to that of the 5 and 9 DB wire suggesting it is negative due to a tip induced charging. The full line scans for the 8 to 15 DB wires presented in Figure S14 clearly indicate that an increased wire length allows for a greater degree of charge distributions within the wires. The increased length means that charges are more effectively screened along the wires resulting in a decoupling of the wire into smaller subunits. As the tip bias is increased, the structure of the DB wire can reconfigure due to the stabilizing polaronic effect from charge injection from the tip. Since the DB wires appear to more easily switch between the various configurations, it makes it difficult to assign a single lattice configuration as was done for DB wires of shorter length.

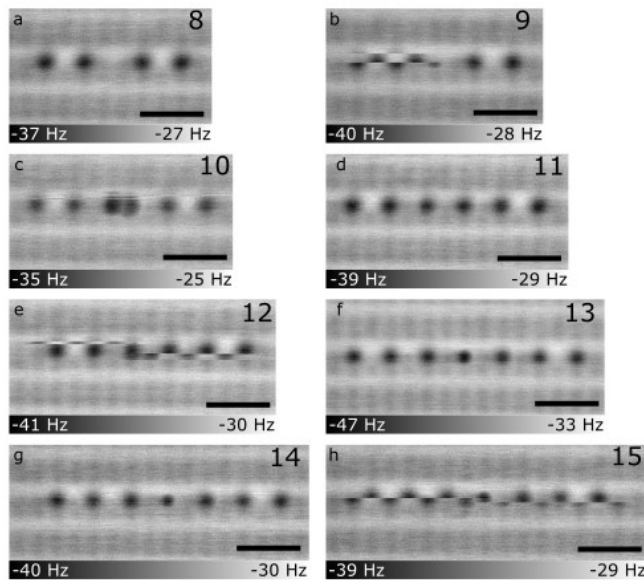


Figure S13. **DB wires of Longer Length.** (a)-(h) $\Delta f(V)$ maps of DB wires of length 8 to 15 as indicated in the top right of each image. All images are taken at 0 V and -300 pm. Scale bar is 1nm.

Wire Length

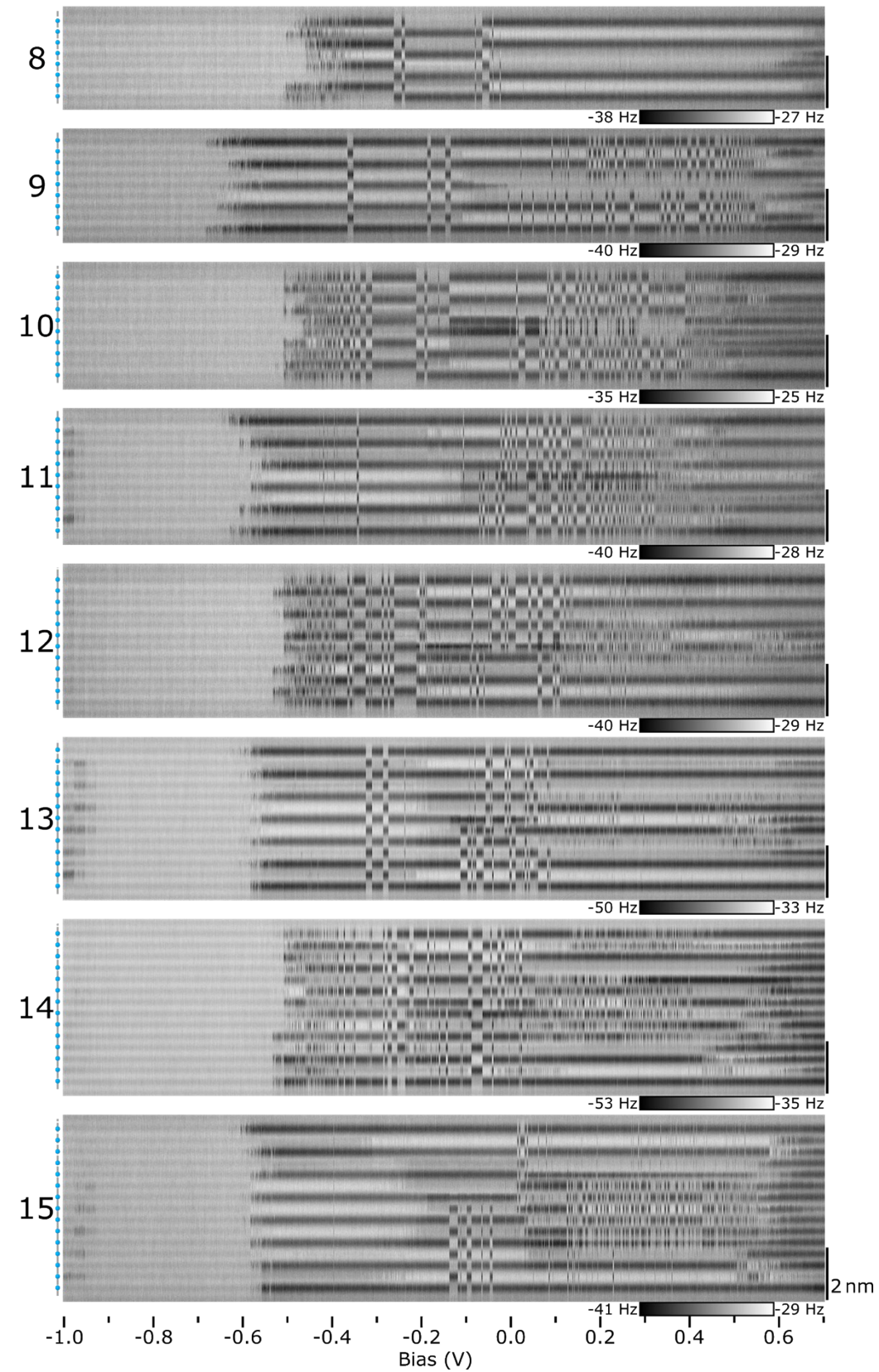


Figure S14. **Charge Distribution Among Longer Wires.** Line scans of DB wires length 8 to 15. Bias increments are 0.02 V with 50 line scans taken at each bias. All line scans were taken at a relative height of -300 pm. The position of DBs within the DB wires is indicated to the left of the line scans in blue.

References

- 1 S. Watanabe, Y. A. Ono, T. Hashizume and Y. Wada, *Phys. Rev. B*, 1996, **54**, R17308–R17311.
- 2 J. Y. Lee, J. H. Cho and Z. Zhang, *Phys. Rev. B*, 2009, **80**, 155329.
- 3 J.-H. Cho and L. Kleinman, *Phys. Rev. B*, 2002, **66**, 235405.
- 4 M. Rashidi, M. Taucer, I. Ozfidan, E. Lloyd and H. Labidi, *Phys. Rev. Lett.*, 2016, **117**, 276805.
- 5 M. Rashidi, E. Lloyd, T. R. Huff, R. Achal, M. Taucer, J. J. Croshaw and R. A. Wolkow, *ACS Nano*, 2017, **11**, 11732–11738.
- 6 H. Kawai, O. Neucheva, T. L. Yap, C. Joachim and M. Saeys, *Surf. Sci.*, 2016, **645**, 88–92.
- 7 J. E. Northrup, *Phys. Rev. B*, 1989, **40**, 5875(R).
- 8 M. Berthe, A. Urbieto, L. Perdigão, B. Grandidier, D. Deresmes, C. Delerue, D. Stiévenard, R. Rurali, N. Lorente, L. Magaud and P. Ordejon, *Phys. Rev. Lett.*, 2006, **97**, 206801.
- 9 S. Godlewski, M. Kolmer, J. Lis, R. Zuzak, B. Such, W. Gren, M. Szymonski and L. Kantorovich, *Phys. Rev. B*, 2015, **92**, 115403.
- 10 R. Pérez, M. C. Payne, I. Štich and K. Terakura, *Phys. Rev. Lett.*, 1997, **78**, 678–681.
- 11 M. Rashidi, W. Vine, T. Dienel, L. Livadaru, J. Retallick, T. Huff, K. Walus and R. A. Wolkow, *Phys. Rev. Lett.*, 2018, **121**, 166801.
- 12 A. Sweetman, S. Jarvis, R. Danza, J. Bamidele, L. Kantorovich and P. Moriarty, *Phys. Rev. B*, 2011, **84**, 85426.
- 13 R. M. Feenstra, Y. Dong, M. P. Semtsiv and W. T. Masselink, *Nanotechnology*, 2007, **18**, 044015.
- 14 J. L. Pitters, P. G. Piva and R. A. Wolkow, *J. Vac. Sci. Technol. B*, 2012, **30**, 021806.
- 15 R. Robles, M. Kepenekian, S. Monturet, C. Joachim and N. Lorente, *J. Phys. Condens. Matter*, 2012, **24**, 445004.
- 16 D. R. Bowler and A. J. Fisher, *Phys. Rev. B*, 2000, **63**, 035310.
- 17 M. Todorovic, A. J. Fisher and D. R. Bowler, *J. Phys. Condens. Matter*, 2002, **14**, L749.
- 18 H. Ness and A. J. Fisher, *Appl. Surf. Sci.*, 2000, **162**, 613–619.
- 19 F. Bird, J. Fisher and R. Bowler, *Phys. Rev. B*, 2003, **68**, 115318.